Photodisintegration of C^{13}†*‡

BARNETT C. COOK§
The Enrico Fermi Institute for Nuclear Studies, The University of Chicago, Chicago, Illinois
(Received November 9, 1956)

The neutron yield functions of C^{12} and C^{13} from bremsstrahlung up to 41 Mev have been measured by using direct neutron detection. The photoproton yield function for C^{13} has also been measured by detecting the B^{12} activity. These yield functions were converted into cross sections (σ) by a slightly modified standard method.

σ for $C^{13}(\gamma,xn)$ exhibits a peak of $\sim$3.7 mb at $\sim$13.5 Mev and the "giant resonance" peak of $\sim$10 mb at $\sim$24 Mev. This latter peak is broad [$\Gamma_{\frac{1}{2}}\approx$10 Mev] in contrast to C^{12} with $\Gamma_{\frac{1}{2}}\approx$3 Mev.

σ for $C^{13}(\gamma,p)B^{12}$ exhibits a broad ($\Gamma_{\frac{1}{2}}\approx$6 Mev) giant resonance peak of 8.8 mb at 25.5 Mev. This large p/n emission ratio cannot be accounted for by statistical considerations.

After a reasonable allowance is made for multiple processes, these two measurements are combined to give the total γ-absorption cross section, σ_{abs}. σ_{abs} of C^{12} is also discussed. Both show a giant resonance peak but $\Gamma_{\frac{1}{2}}(C^{13})\gg\Gamma_{\frac{1}{2}}(C^{12})$ whereas the integrals of σ_{abs} over the resonance are approximately equal. The idea that core excitation is responsible for the giant resonance is supported by the approximate equality of the resonance energies of C^{12} and C^{13}, but the remarkable difference in the width of these resonance peaks suggests a strong dependence of the absorption process on the ground-state configurations. The peak at 13.5 Mev found in $C^{13}(\gamma,n)$ is still present in σ_{abs} and hence is not due to competition, but represents a "pygmy resonance."

During this work a new half-life for B^{12} was obtained: $(18_{-1.3}^{+1.5})$ msec.

I. INTRODUCTION

ALTHOUGH the (γ,n) and (γ,p) cross sections are known for many nuclei,[1–3] the total photon absorption cross section (σ_{abs}) has been measured for only a few light elements. While for heavy elements σ_{abs} is essentially known once $\sigma(\gamma,n)$ is known since the latter predominates; for light elements, on the contrary, the (γ,p) and (γ,n) cross sections have comparable magnitudes.[4] Cross sections for other processes such as (γ,d) and (γ,pn) usually give unimportant contributions to the total cross section although in a few instances these processes must also be considered. Thus at least $\sigma(\gamma,p)$ as well as $\sigma(\gamma,n)$ must be measured for low-Z elements to obtain σ_{abs}. Although both cross sections are known for some light elements, so far we have no knowledge of σ_{abs} for the very interesting case of two nuclides differing by only one mass number. The pair C^{12}, C^{13} belong to this category and are amenable to experimental investigation since $C^{12}(\gamma,n)C^{11}$ has been investigated repeatedly by the activation method[5–9] and by direct neutron counting,[1,2,10] and the cross section $C^{12}(\gamma,p)C^{11}$ has been measured by detecting the protons directly.[11] Enriched C^{13} has become available in sufficient amounts (grams) that the photoneutrons can be counted directly by standard techniques and the B^{12} produced by the (γ,p) process detected conveniently.

Measurements of σ_{abs} for this particular pair of nuclides seems to be especially attractive as σ_{abs} of C^{12} is in some ways unique. For example, the giant resonance peak is abnormally narrow and the cross section above the peak large. A wide resonance for C^{13} would suggest that the narrow resonance in C^{12} may be related to the closing of the $p_{\frac{3}{2}}$ subshell. Thus a measurement of the C^{13} cross section might bring out special ground state effects on photonuclear reactions similar to those reported at the closing of the neutron shell at the magic number 50.[12]

Aside from the previous considerations, C^{13} itself appears to be an interesting choice for study from several other viewpoints. It has been suggested that the well known giant resonance peak in (γ,n) cross sections occurs at an energy better correlated with the threshold energy for neutron emission than with the mass number A itself.[13] Although recent work at the University of Pennsylvania[14] has shown that this suggestion is in general unfounded, some small correlation of the energy (E_p) of peak in $\sigma(\gamma,n)$ with the threshold is to be expected from statistical arguments alone,[15] even if the

† Research supported by a joint program of the Office of Naval Research and the U. S. Atomic Energy Commission.

* Submitted to the Faculty of the Department of Physics, the University of Chicago, in partial fulfillment of the requirements for the Ph.D. degree.

‡ A preliminary report of this work has been published: B. C. Cook and V. L. Telegdi, Bull. Am. Phys. Soc. Ser. II, **1**, 63 (1956); Cook, Penfold, and Telegdi, Phys. Rev. **104**, 554 (1956). These reports will be referred to as I and II, respectively.

§ Present address: Department of Physics, University of Pennsylvania, Philadelphia, Pennsylvania.

[1] Montalbetti, Katz, and Goldemberg, Phys. Rev. **91**, 659 (1953). This paper contains a useful table of the properties of photoinduced reactions measured by the activity of the residual nucleus and also direct neutron counting.

[2] R. Nathans and J. Halpern, Phys. Rev. **93**, 437 (1954). This paper summarizes some results for monoisotopic elements by direct neutron counting.

[3] E. V. Weinstock and J. Halpern, Phys. Rev. **94**, 1651 (1954). This paper lists the photoproton yields for many nuclides near 22 Mev.

[4] S. Johansson, Phys. Rev. **97**, 1185 (1955).

[5] Barber, George, and Reagan, Phys. Rev. **98**, 73 (1953).

[6] L. Katz and A. G. W. Cameron, Can. J. Phys. **29**, 518 (1951).

[7] R. Sagane, Phys. Rev. **84**, 587 (1951).

[8] K. Strauch, Phys. Rev. **81**, 973 (1951).

[9] L. Marshall, Phys. Rev. **83**, 345 (1951).

[10] L. W. Jones and K. M. Terwilliger, Phys. Rev. **91**, 699 (1953).

[11] J. Halpern and A. K. Mann, Phys. Rev. **83**, 370 (1951).

[12] P. Yergin and B. Fabricand, Phys. Rev. **100**, 1269 (1955).

[13] Katz, Baker, Haslam, and Douglas, Phys. Rev. **82**, 271 (1951).

[14] R. Nathan and P. Yergins, Phys. Rev. **98**, 1296 (1955).

[15] Santos, Goldemberg, Silva, Borrello, Villaca, and Lopes, Anais acad. brasil. cienc. **27**, 437 (1955).

energy E_p of the giant resonance in σ_{abs} is completely independent of all thresholds for particle emission. A measurement of the $C^{13}(\gamma,n)$ cross section would yield further information about the threshold dependence of E_p in $\sigma(\gamma,n)$ as the (γ,n) thresholds of C^{12} and C^{13} are 18.72 Mev and 4.95 Mev, respectively. Moreover the threshold dependence of E_p in σ_{abs} has never been measured previously by comparing nuclides of similar masses but differing widely in binding energies.

The $\sigma(\gamma,n)$ of C^{13} near threshold is interesting in view of the success of a simple model[16,17] for Be^9 in explaining both the energy dependence of the cross section $Be^9(\gamma,n)Be^8$ and the angular distribution of the photoneutrons near threshold.[18,19] In this model one assumes a direct photoemission of the unpaired neutron from Be^9 described as a core plus a single particle in an orbit. In some respects such a model might be expected to approximate reality more closely for C^{13} than for Be inasmuch as the core of C^{13}, i.e., C^{12}, is closed in $j-j$ coupling while it is unfilled for Be^9. On the other hand, the existence of a 2^+ state in C^{12} at 4.43 Mev, some 500 kev below the $C^{13}(\gamma,n)C^{12}$ threshold, casts doubt about the correctness of the model even near threshold. A measurement of $\sigma(\gamma,n)$ can establish the useful energy range of validity of this model for C^{13}.

On the basis of the preceding considerations we decided to determine $\sigma(\gamma,n)$ and $\sigma(\gamma,p)$ for C^{13} in this laboratory. The (γ,n) yield from bremsstrahlung was measured as a function of betatron energy at one Mev intervals from 6 Mev to 41 Mev by direct neutron counting. The (γ,p) yield was determined analogously at one Mev intervals from 17 to 32 Mev, and at larger intervals to 45 Mev by detecting the 13.43-Mev β^- from B^{12} in GM counters. Both yield functions were converted to cross sections using slight modifications of standard methods.[20] Neglecting the $(\gamma,2p)$ process and making reasonable assumptions about the $(\gamma,2n)$ and (γ,pn) processes, the two cross sections were then combined to give an approximation to $\sigma_{abs}(E_\gamma)$. For reasons to be discussed later, we confine our derived cross sections to $E_\gamma \leq 35$ Mev, although the yield functions are presented up to 41 Mev.

II. EXPERIMENTAL PROCEDURE COMMON TO (γ,n) AND (γ,p)

Betatron Performance

A discussion of the performance of the University of Chicago betatron on obtaining yield-functions is in order as the two previous reports[21–22] from this laboratory containing activation functions did not discuss this point and relied heavily upon this work for their validity. The betatron energy scale must be linear and accurately calibrated to obtain meaningful yield functions. This scale is determined here by the integral of the voltage induced in a turn around the centerpiece of the betatron.[23] The linearity of the electron energy (the upper limit of the bremsstrahlung, E_0) as a function of this integrated voltage was checked by magnetic field measurements at 50 and 100 Mev and by measuring the 10.7 ± 0.1 Mev threshold[24,25] of $Cu^{63}(\gamma,n)Cu^{62}$, and the 19.55-Mev "break"[26,27] in the $C^{12}(\gamma,n)C^{11}$ activation curve. The nominal energy scale of the betatron was determined by a field measurement at 100 Mev. The latter two activation measurements determine the absolute energy scale. The Cu^{63} threshold was found at a nominal energy of 10.5 ± 0.1 Mev, and the C^{12} break at 19.5 ± 0.1 Mev. Thus the nominal energy scale of the betatron is linear and correctly calibrated to within ±200 kev for all energies used in this experiment.

In the actual operation of the betatron the integrated voltage mentioned above is compared with an adjustable reference voltage calibrated in Mev. An ejection trigger pulse is generated when the difference between these two voltages is zero. X-rays are then obtained within 30–70 μsec following this trigger pulse depending upon the electron energy. The stability of E_0 is determined by the stability of the comparison circuit and the time jitter in the electronics following the trigger pulse. The over-all stability of E_0 was checked by repeated measurement of the ratio of the $C^{12}(\gamma,n)C^{11}$ and $Cu^{63}(\gamma,n)Cu^{62}$ yields at 22 and 38 Mev. The larger fluctuations in this ratio, which is a strong function of energy at 22 Mev and almost independent of energy at 38 Mev, at the lower energy can be attributed to an energy instability of ±50 kev. For runs of the order of an hour or less, such as used in the present experiment, a conservative estimate for the stability of E_0 is about ±100 kev.

Preparation and Description of Samples

The C^{13} sample was obtained in the form of finely divided charcoal by reducing enriched[28] (64.8%) $BaCO_3$ to elemental carbon. Libby's method,[29] in which CO_2 is reduced to C by using Mg in a Fe tube, was used for this. It was found that the following modifications improved the purity of the sample and increased the yield; (1) operating at a CO_2 pressure of $\frac{1}{3}$ atmospheres or less in order to avoid excessive heating of the iron tube with

[16] E. Guth and C. J. Mullin, Phys. Rev. **76**, 234 (1949); **76**, 682 (1949).
[17] T. Sexl, Acta Phys. Austriaca **3**, 277 (1949).
[18] B. Hamermesh and C. Kimball, Phys. Rev. **90**, 1063 (1953).
[19] R. Nathans and J. Halpern, Phys. Rev. **92**, 940 (1953).
[20] A. S. Penfold and J. E. Leiss, Phys. Rev. **95**, 637(A) (1954).
[21] C. S. del Río and V. L. Telegdi, Phys. Rev. **90**, 439 (1953).
[22] L. Meyer-Schützmeister and V. L. Telegdi, Phys. Rev. **104**, 185 (1956).
[23] In principle this method is superior to the method used at other laboratories where the current in the exciting coils of the betatron is integrated. Katz, McNamara, Forsyth, Haslam, and Johns, Can. J. Research **A28**, 113 (1950).
[24] M. Birnbaum, Phys. Rev. **93**, 146 (1954).
[25] Sher, Halpern, and Mann, Phys. Rev. **84**, 387 (1951).
[26] B. M. Spicer and A. S. Penfold, Phys. Rev. **100**, 1375 (1955).
[27] Katz, Haslam, Horsley, Cameron, and Montalbetti, Phys. Rev. **95**, 464 (1954). We have identified the 19.3 Mev of Katz with the 19.55 Mev break of Spicer and Penfold.
[28] Obtained from the Eastman Kodak Company.
[29] W. F. Libby, *Radiocarbon Dating* (University of Chicago Press, Chicago, 1952), pp. 42–51.

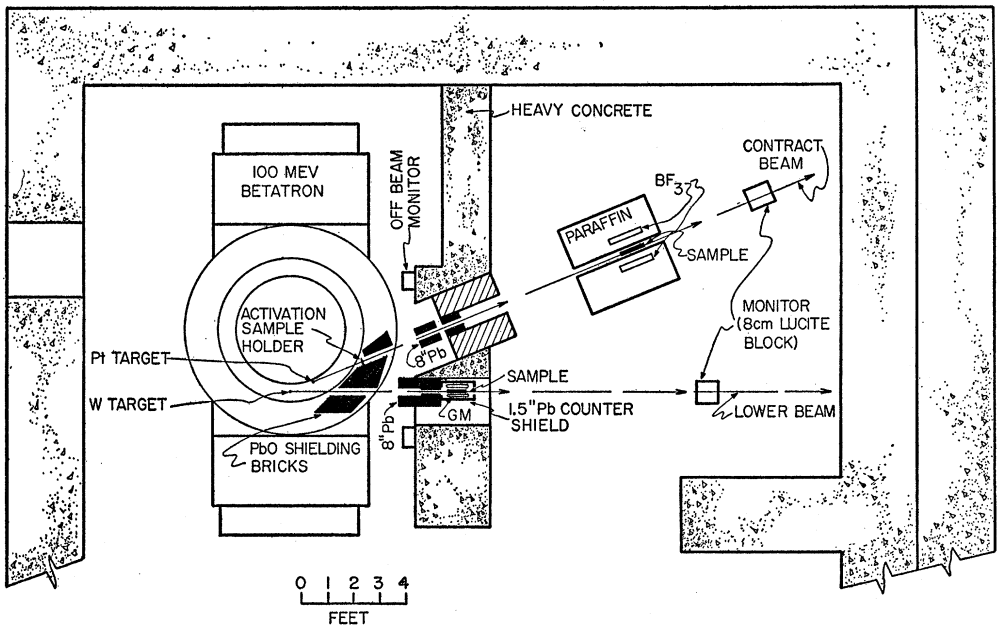

FIG. 1. Plan view of betatron room showing physical arrangement for the (γ,n) and (γ,p) experiments.

ensuing formation of carbides; (2) using carbon-free iron tubes to prevent isotope dilution. Yields approaching 80% were obtained. A C^{12} sample was prepared at the same time for comparison measurements. The weight and composition of the C^{12} and C^{13} samples are indicated in Table I.

It was found that heating the charcoal samples so obtained to 1000°F in vacuum and then letting them cool in hydrogen made them stable against adsorption of air and other gases. In fact the samples finally used in this experiment gained $\approx 1\%$ in weight over a period of 9 months. The samples were packed in one-mil-thick polyethylene "tubes," roughly cylindrical in shape and $\frac{3}{8}$ inch in diameter. The C^{13} tube was about 8 inches long; that containing C^{12} about 9 inches.

Experimental Arrangement

Figure 1 shows a general plan view of the experimental arrangement. Of the four x-ray beams available, the "contract" beam was used for the photoneutron work and the "lower" beam for the photoproton work. The equipment used for the (γ,n) and (γ,p) measurements was shielded from the betatron doughnut by a 3 ft heavy concrete (Fe-loaded) wall and by 2×2×4-inch PbO bricks (8 g/cm³) between the field coils. The "contract" beam from a 10-mil Pt target was defined to 0.2° divergence with 8 inches of Pb. It then passed successively through a second, somewhat wider 8-inch Pb collimator, a 4×4-inch channel in the Fe filling the shield wall, a 1.5-inch diameter passage in the neutron counter housing, and finally struck the monitor. The defining collimator was at 128 cm, the sample at 386 cm, and the monitor at 689 cm from the target. The (γ,p) equipment was located in the window of the shield wall used for the "lower" beam. This beam was collimated in 8-inch Pb to 1-inch diameter at the sample, 194 cm from the target (22-mil W wire). Lead was used to shield the equipment adequately. The equipment was aligned initially with respect to the beams photographically: the position of the latter was found to be independent of energy from 10–50 Mev. The sample position was checked frequently during the course of the experiment. The electron contamination of the x-ray beam was found to be negligible.

The monitor usually used in both experiments was a 500-mr thimble ionization[30] chamber set in 8-cm cube of Lucite. Its response to Co^{60} γ rays agrees with that of a 25-r Victoreen chamber such as is often used in photonuclear work; for 50-Mev bremsstrahlung the response differed by 2.5%. No saturation effects were found at the highest beam intensities used.

TABLE I. Chemical composition and weights of C^{12} and C^{13} samples.

(a) Chemical composition

Constituent	%
C	93.1
H	2.3
Ash (Mg, Fe, Si, Al)	1.7
Others (volatile)	2.9

(b) Weights (grams)

	C^{13} sample	C^{12} sample
Sample	1.738	1.930
Tube	*0.315*	*0.363*
Total	2.053	2.343
Total C	1.888	2.155
Total C^{13}	1.078	0.026
Total C^{12}	0.810	2.129

[30] Landsverk Electrometer Company "Gold Band" Roentgen Meter Model *L*-110.

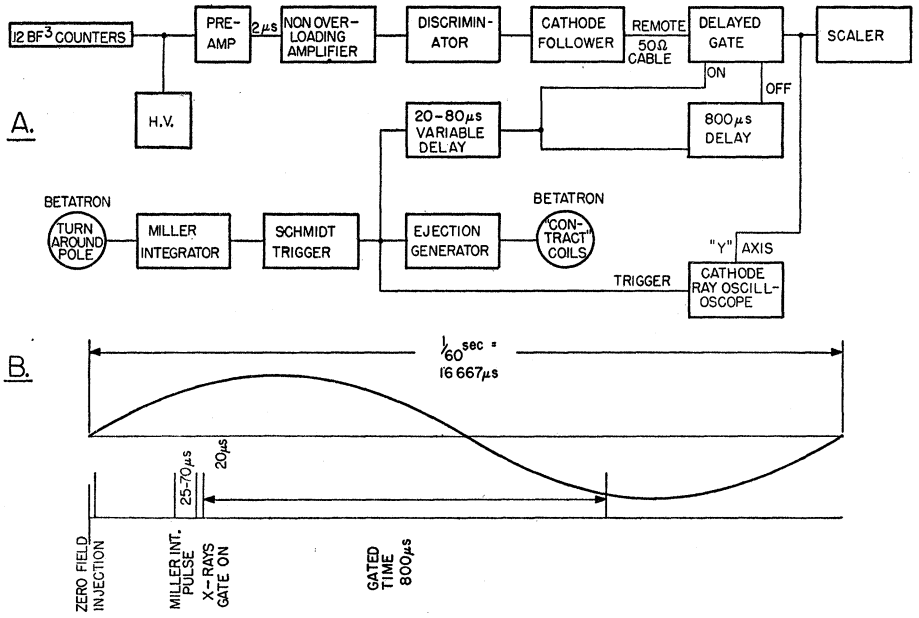

FIG. 2. (A) Block diagram of the electronics used for the (γ,n) experiment. (B) Schematic representation of the timing.

III. (γ,n) EXPERIMENT

Neutron Detection

A neutron detection system based upon Halpern's design[31] was used. Twelve enriched $B^{10}F_3$ counters (1-inch diameter, 10-inch effective length) were embedded in paraffin on a cylinder of 13-cm radius concentric with the sample. This assembly was shielded by 8-inch paraffin and $\frac{1}{32}$-inch Cd on all sides except on the betatron side where 24 inches of paraffin were used. The C^{12} and C^{13} samples were centered in two Synthane tubes (1.5-inch o.d.) which fitted closely into the counter housing and were reproducibly positioned.

Figure 2(A) shows a block diagram of the electronics used and Fig. 2(B) depicts the timing used schematically. Since a complete description of the operation has been given elsewhere,[31] we believe that only the slight differences need be mentioned. The 12 counters, operated in parallel at 1900 v with an input sensitivity of 1.5 mv, exhibited a plateau for Ra-Be neutrons (2%/100 v) of 250 v length. The non-overloading amplifier[32] (Chase-Higinbotham design) is required to insure quick recovery of the counting system after the beam pulse. The delay after ejection must be variable as the beam delay after the ejection trigger depends upon the energy. An oscilloscope was used to set this delay and monitor the gate operation.

The counting efficiency (about 6%) for Ra-Be neutrons was stable (about one percent) during the course of the experiment. All timing was determined using a calibrated oscilloscope. The duty cycle for counting measured by counting a random neutron source and from the measured gate length agreed. The gate triggering was completely reliable and the gate delay and length were stable.

[31] Halpern, Mann, and Nathans, Rev. Sci. Instr. **23**, 678 (1952).
[32] Beva Laboratory Model 152.

Procedure

At least three independent runs were made at 1-Mev intervals from 6 to 30 Mev. From 30 to 41 Mev only one run was made at each yield point using a 5-r thimble for monitoring. The energy sequence was selected to minimize systematic errors. Depending upon the energy, running times varied between 2 hr and 10 min; above 20 Mev all runs were 10 min as the approximately equal beam intensity was used to keep pileup errors completely negligible. A no-sample run was taken after each C^{13} run to determine the background. At 30 Mev the sample to background ratio was 9/1 and improved at both higher and lower energies.

Yield Function

A plot of the yield points $Y_n(E_0)$ (less background and corrected to monitor response at NTP) so obtained *versus* energy E_0 is shown in Fig. 3. Their errors, as constructed from the reproducibility of the data and counting statistics at $E_0 \approx 25$ Mev, are about $\pm 2.7\%$ for an individual yield point or about 1.5% for the average of three runs. The deviations (about $\pm 2\%$) of the points from a smooth curve in excess of counting statistics ($\sim 1\%$) probably arise in monitoring difficulties.

The absolute yield is based upon Katz's[1] value[11] of 1.7×10^8 neutrons/mole-100 r for Cu at 18 Mev. In practice the yield from Cu was compared to that from

[11] *Note added in proof.*—Professor Katz has informed me that this value should be reduced by 10%. Thus all the yields and cross sections described in this paper based upon this normalization must be similarly reduced (private communication).

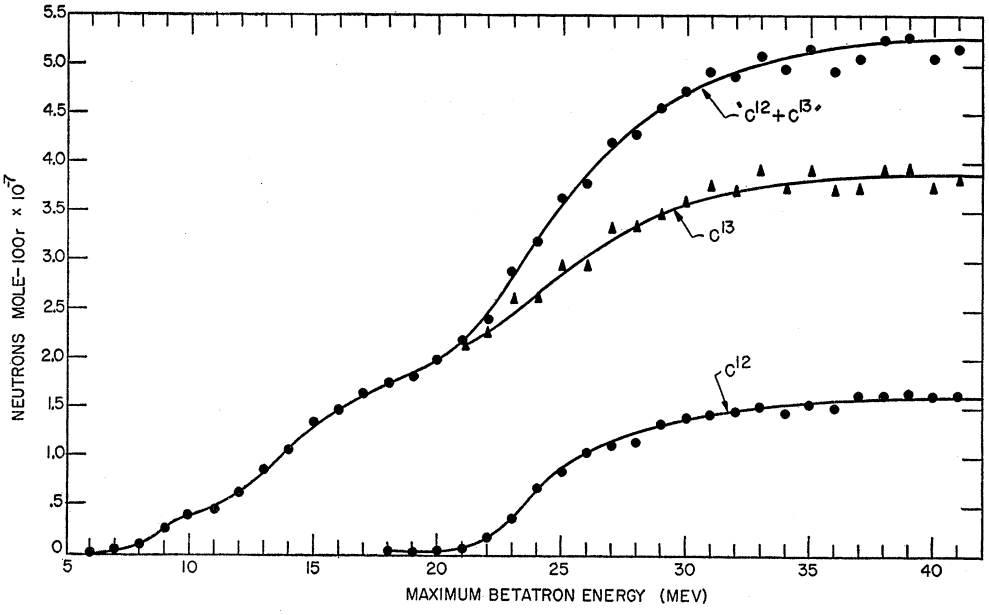

FIG. 3. $C^{13}(\gamma,xn)$ and $C^{12}(\gamma,xn)$ yield functions up to 41 Mev.

the samples at 30 Mev by using a more divergent (0.4°) beam than that used for the yield function which encompassed the samples. The ratio of Cu yields at 30 Mev and 18 Mev was then determined carefully. Corrections were applied for the finite length of the samples. Although the beam did not strike the entire monitor no

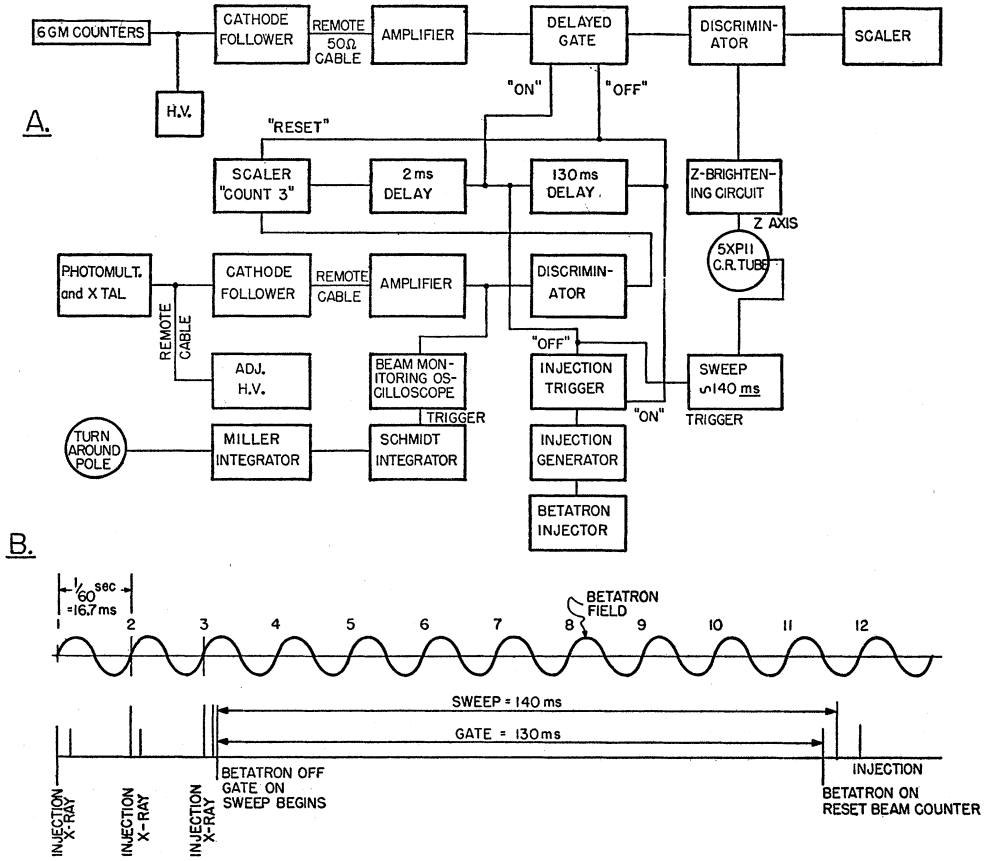

FIG. 4. (A) Block diagram of the electronics used for the $C^{13}(\gamma,p)B^{12}$ experiment. (B) Schematic representation of the timing.

corrections to the monitor reading need be applied as the measured correction was independent of beam energy. Table II lists all factors entering this normalization.

$Y_n(E_0)$ of C^{13} (corrected for the C^{12} in the sample) at 22 Mev is $(2.3\pm0.2)\times10^7$ neutrons/mole-100 r while the $Y_n(E_0)$ of C^{12} is $(1.5\pm0.2)\times10^6$ neutrons/mole-100 r. The Saskatchewan group[1] obtained 3.5×10^6 neutrons/mole-100 r and Price and Kerst[33] 0.7×10^6 neutrons/mole-100 r for C^{12} at this energy. A 500-kev shift in the energy scale used at each laboratory will bring the measurements into agreement. These discrepancies justify our redetermination of the $Y_n(E_0)$ of C^{12} to correct the sample yield for its C^{12} content; for, if published C^{12} yield functions were used, the C^{13} yield function would have been considerably distorted. The large discrepancies in published photonuclear yields and cross sections has been stressed before by the Pennsylvania group.[12]

The (γ,n) cross section will be discussed in a later section.

TABLE II. Factors for absolute normalization of $Y_n(E_0)$.

	C^{12}	C^{13}
1. Assumed Cu yield at 18 Mev	1.7×10^8	1.7×10^8 neutrons/mole-100 r
2. Ratio of Cu yield at 30 Mev to yield at 18 Mev	2.17	2.17
3. Ratio: moles Cu/moles C	0.0487	0.1058
4. Correction for finite length of samples	0.82	0.85
5. C yield for 0.4° beam/C yield for 0.2° beam	1.36	1.26

IV. $C^{13}(\gamma,p)B^{12}$

Equipment

The short-lived activity of B^{12} is readily detected in GM counters by appropriately cycling the betatron output. Since the half-life ($\approx$25 msec) of B^{12} and the repetition time of the betatron (16.7 msec) are comparable, about $\frac{7}{8}$ of the saturated activity from B^{12} can be produced in three injection cycles while the activity is practically gone after nine more cycles.

Six GM counters[34] were arranged symmetrically about the sample to detect the decay. The counters were positioned by iron spacers exclusively as preliminary experiments had shown that other materials lead to troublesome backgrounds from neutron capture activities. Figure 4(A) shows a block diagram of the electronics used to program the betatron and record the GM counts in the above cycle; the sequence of events during the latter is illustrated in Fig. 4(B). If a betatron injection pulse occurs at $t=0$, a beam pulse follows within the next $\frac{1}{4}$ cycle of the magnetic field, the exact time depending upon the energy. The pulse is detected in a small NaI(Tl) crystal and photomultiplier. After appropriate amplification and shaping it is counted in the scaler "count 3." The cycle continues until 3 beam pulses are recorded, then [shortly after cycle 3 on Fig. 4(B)] the injection trigger is turned off so that no electrons will be accelerated in the betatron until the trigger is again initiated. Two milliseconds later the delayed gate is opened, allowing GM counts to be recorded in the scaler. After 130 msec the gate closes, the scaler "count 3" is reset, and the injection trigger is turned on. When the betatron is properly phased, electron injection occurs and the cycle is renewed.

The counts recorded by the scaler are not necessarily due solely to B^{12} activity and hence are not sufficient for yield measurements. In fact a complete decay curve must be obtained at each energy (E_0) for which the yield is to be measured. For millisecond half-lives a conventional way to do this is to display each decay

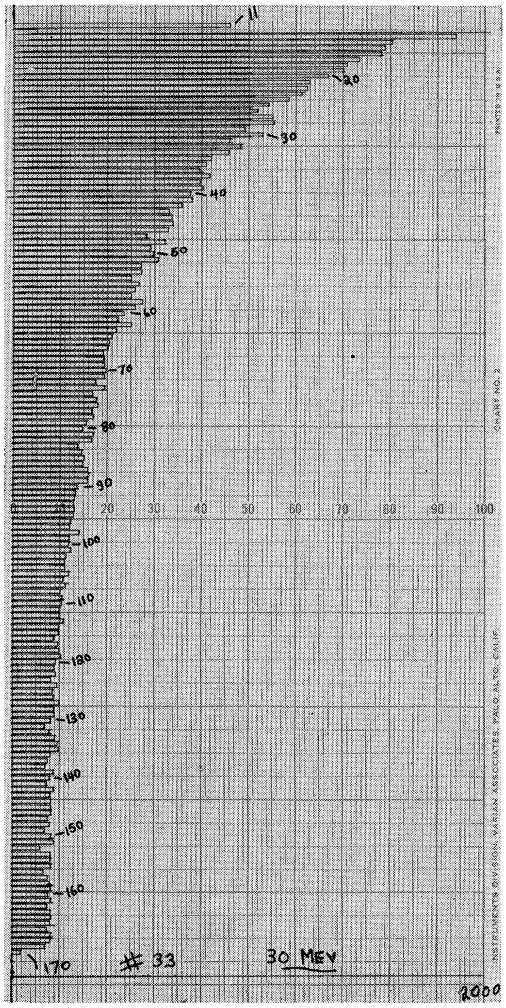

FIG. 5. Reproduction of a typical Varian Record Chart showing number of G-M counts as a function of channel number. (1 channel $\approx$1 msec) Run was taken at $E_0\approx30$ Mev. Full scale represents 2000 counts. The separation of the decay into a short-lived component (B^{12}) and a background is apparent.

[33] G. A. Price and D. W. Kerst, Phys. Rev. **77**, 806 (1950).
[34] Eck and Krebs—type 1108.

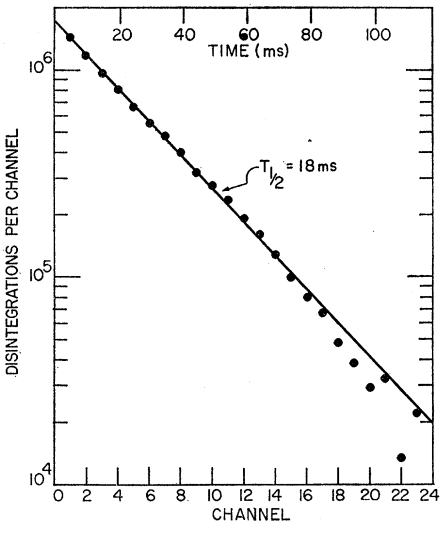

FIG. 6. Decay of B^{12}.

event on an oscilloscope with linear sweep and to photograph the screen. In this experiment the oscilloscope was an adaptation of a Zaffarano type[35] "dot analyzer"; it is indicated in Fig. 4(A) as the 5XP11 C.R. tube. Its horizontal sweep, started when counting begins and defining a time axis, is derived from the sweep circuitry of a strictly linear oscilloscope.[36]

The Z-brightening circuit for the 5XP11, normally inoperative, is turned on by the output of a discriminator following the GM counters so that each accepted GM count appears as a flash at an appropriate point on the time axis. The sequence of flashes is photographed as dots (10-mil diameter) on Linograph Ortho film using a Fairchild Type 314 camera (Summicron F:2 lens) with 1:2 minification. Since the film was advanced at 9 inches/min, successive sweeps appear displaced vertically along the film. To assure satisfactory uniformity of dots across the film, push-pull sweep deflection of the 5XP11 was found absolutely necessary. The sweep was made about 10 msec longer than the gate (130 msec) and returned automatically to its zero during the bombardment of the sample. In tests the equipment followed the above cycle without exception (about 8000 cy).

An additional oscilloscope, indicated in Fig. 4(A), was used to monitor the beam to ascertain that acceleration occurred after each injection pulse and that the intensities of the three pulses were equal on the average. To obtain this condition it proved necessary to sacrifice beam intensity as the capture conditions into a stable betatron orbit appear to be too critical for stable pulsed operation at the optimum injection phase.

The film was read by using a replica of the automatic film scanner developed at Iowa State College[35] for use in conjunction with the "dot analyzer." This scanner counts the number of dots in 5-mil channels across the film; each channel corresponding to about 1 msec under the conditions of operation used. The number of counts in each channel was converted to a voltage and then recorded on a chart using a Varian recorder advanced after the completion of each channel scan. In this way decay curves were obtained at each beam energy E_0. A typical chart, obtained at 30 Mev, is reproduced in Fig. 5, where full scale corresponds to 2×10^3 counts/channel. A short half-life component and a background are evident.

Absolute time calibration was achieved by recording on each film dots generated by counting the 60-cycle line frequency. The sweep length was stable to one channel in 160 channels and the zero position did not drift more than one channel during any given run. This drift introduces an error of about 1 msec in the definition of zero time, thus affecting absolute yield determinations but not the half-life measurement. As a check a random source was used to obtain approximately uniform dot density across the film. This showed variations in the light output across the 5XP11 screen produced systematic deviations (about 2.5%) in the efficiency for counting dots in certain channels through changes in dot size. However the net effect upon events monotonically distributed in time can be neglected.

Identification of Activity

The assignment of the short-lived component to B^{12} was verified (1) by an absorption measurement [half-thickness of (1.3 ± 0.2) g/cm^2 Al corresponding to $E_{max}\approx15$ Mev] (2) a threshold energy of about 18 Mev, and (3) the absence of a short half-life activity when a C^{12} sample was substituted for C^{13}.

Half-life of B^{12}

All data were grouped into bins of six channels beginning with the ninth channel from zero time as a short-lived (1 msec) neutron-induced activity was present. All data in runs with $E_0\geqslant26$ Mev were combined and fitted by least squares to the expression

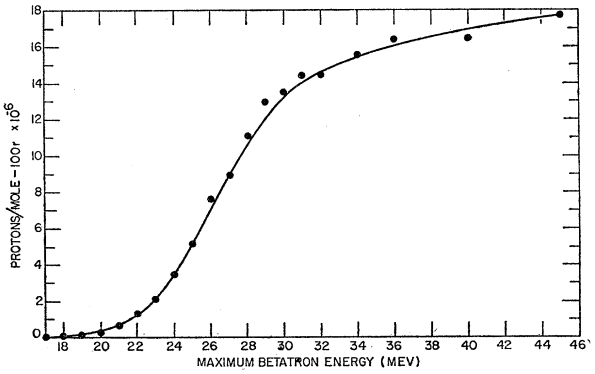

FIG. 7. $C^{13}(\gamma,p)B^{12}$ yield function up to 45 Mev.

[35] Hunt, Rhinehart, Weber, and Zaffarano, Rev. Sci. Instr. **25**, 268 (1954).
[36] Tektronix Model 541.

$A+B\exp[-\lambda n]$, where n is the bin number. This best fit decomposition of the decay curve is shown in Fig. 6, in which A has been omitted.

A half-life of $(18_{-1.3}^{+1.5})$ msec was obtained, and is to be compared with 22 msec[37] and 27 msec[38] reported for B^{12} from earlier work. This result was subjected to the following tests: (1) points of the decay curve corresponding to the first half-life were omitted; (2) runs at 26, 32, and 45 Mev, having widely different activity/background ratios, were separately decomposed; (3) a series of runs were recorded with a sweep of 1.5 msec/channel. The analysis of all three sets of data was consistent with a half-life of 18 msec. The error quoted above is not statistical (over 7×10^6 disintegrations were recorded), but rather reflects variations in the efficiency for counting dots across the film.

Yield Function Determination

Two runs were made at all E_0 (at 1-Mev intervals) to 32 Mev and at wider energy intervals up to $E_0=45$ Mev. Al (0.27 g/cm) was interposed between the sample and counters to minimize the C^{11} background from $C^{12}(\gamma,n)C^{11}$. For $E_0>32$ Mev, the beam intensity was reduced to avoid pileup of dots.

Each decay curve was decomposed by least-squares fitting into an 18.0-msec activity and a constant background. The ratio activity/background was 1/1 at 22 Mev and 12/1 at the highest energy. From the consistency achieved in runs at the same E_0, we estimate a relative error of about $\pm4\%$ for each yield point (Fig. 7) with $E_0\geqslant25$ Mev.

Table III lists the factors used to convert the raw experimental data (counts/channel in bin No. 0 per roentgen) to absolute yields $Y_p(E_0)$. Most of these factors are self-explanatory. Correction (3) assumes the x-ray intensity is on the average the same for each successive pulse of a cycle. Since reproducible yields were obtained although the betatron was operated in various runs with different injection phases, this assumption seems justified. Correction (4) is obtained from an experimental absorption curve. The axial dependence of the counting efficiency was determined by using a pointlike P^{32} and Y-Sr^{90} sources. These same

TABLE III. Factors of absolute normalization of $Y_p(E_0)$.

1. Correction to actual time zero (−8.6 msec)	1.392
2. Correction for bin length (4.95 msec)	1.098
3. Decay during bombardment (3 cycles)	1.662
4. Absorption in samples, counters and 1 mm Al	1.16
5. $1/r^2$ correction of monitor	0.152
6. Mean life in channels $(18_{-1.3}^{+1.5}$ msec)	5.26
7. Moles C^{13} $(0.0829)^{-1}$	12.06
8. Central efficiency of counters 85% 6 of 8 counters used 75%	1.567
9. Correction for finite length of sample	1.689

[37] P. Bretonneau, Compt. rend. **236**, 913 (1956).
[38] J. V. Jelley and E. B. Paul, Proc. Camridge Phil. Soc. **44**, 133 (1946).

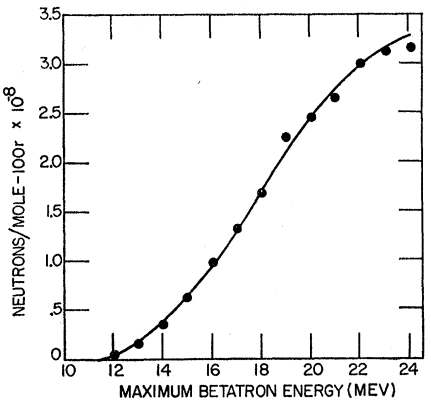

FIG. 8. $Cu^{63}(\gamma,xn)$ yield function. Curve is taken from Montalbetti *et al.* (reference 1).

measurements were used to determine the effective length of the counters and thus the efficiency for a centrally located point source. This calculated efficiency agreed (within 1.5%) with one obtained using a P^{32} source[39] calibrated by 2π counting[40] if appropriate corrections for backscattering and the absorption of P^{32} in the counter walls are made. Since the absorption corrections are small for B^{12}, the calculated efficiency was used.

The estimated absolute accuracy for $Y_p(E_0)$ $(E_0>25$ Mev) is 12.5%. $T_{\frac{1}{2}}$ of B^{12} is the factor limiting the accuracy of $Y(E_0)$.

In Fig. 7 we see that $Y_p(E_0)$ does not begin to rise rapidly up to 22 Mev, 5.5 Mev above threshold, in marked contrast to the (γ,n) yield (Fig. 3) which again increases near 18 Mev after a low-energy contribution to the yield. A displacement of $Y_p(E_0)$ relative to $Y_n(E_0)$ has been found in other nuclei such as A^{40},[41] and perhaps Mg^{25}, Si^{29}, and Si^{30}.[42]

V. CONVERSION OF YIELDS TO CROSS SECTIONS

Spectrum

The (γ,n) and (γ,p) yield functions $[Y_n(E_0)$ and $Y_p(E_0)]$ depend upon the respective cross sections, the monitor response, and the photon spectrum. The latter was assumed to be the integrated over angles bremsstrahlung spectrum of Schiff[43] modified for target and doughnut absorption. The beams used in these experiments give for other reactions, yields which agree closely with those from other laboratories. As an example, Fig. 8 shows the $Cu(\gamma,xn)$ yield obtained here; the smooth curve indicated is taken from Montalbetti

[39] I am indebted to the Argonne Cancer Research Hospital for the P^{32} and Sr-Y^{90} solutions used to prepare the sources. The nominal calibration of the P^{32} solution (as supplied from Oak Ridge) agreed to within 1% with that obtained by 2π counting performed here.
[40] Nader, Hager, and Setter, Nucleonics **12**, 29 (1954).
[41] McPherson, Pederson, and Katz, Can. J. Phys. **32**, 593 (1954).
[42] Katz, Haslam, Goldemberg, and Taylor, Can. J. Phys. **32**, 580 (1954); see however reference 14.
[43] L. I. Schiff, Phys. Rev. **83**, 252 (1951).

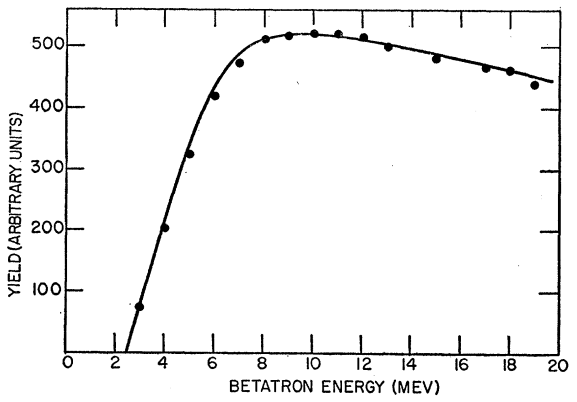

FIG. 9. D$(\gamma,n)p$ yield function. The curve is obtained from the theoretical D$(\gamma,n)p$ cross section and the assumed bremsstrahlung spectrum. The good agreement is evidence that the x-ray spectrum used is not significantly distorted.

et al.[1] However this check supplies little evidence that the spectrum is undistorted below 10 Mev. As an additional check the (γ,n) yield from deuterium (as paraffin) was measured as a function of E_0. The result is shown in Fig. 9. The curve is a theoretical yield obtained by folding the D(γ,n)H cross section[44] into the assumed spectrum and normalized to the experimental yield point at 8 Mev. A further assumption that the detection efficiency for neutron is independent of neutron energy is implicit in this calculation. The correctness of the assumptions appears to be borne out by the excellent agreement.

The response of a thimble embedded in an 8-cm Lucite block for modified bremsstrahlung[45] was recalculated using a revised value of 33.5 ev[46] for W (the energy loss per ion pair in air). The materials modifying the beam by absorption are listed in Table IV; the absorption coefficients were taken from a report by White.[47] The resulting response function [in units of (esu/cm^3)/(erg/cm^2)] is about 10% smaller than that used previously, which entails a corresponding reduction of all absolute cross sections obtained from yields monitored by ionization.[48] Although the agreement among reported cross sections is improved by the above correction, 20% discrepancies[49] are still reported.

[44] J. M. Blatt and V. F. Weisskopf, *Theoretical Nuclear Physics* (John Wiley and Sons, Inc., New York, 1952), p. 609. This cross section agrees well with experiment. See, e.g., Barnes, Carver, Stafford, and Wilkinson, Phys. Rev. **86**, 559 (1952).

[45] L. Katz and A. G. W. Cameron, Can. J. Phys. **29**, 518 (1951).

[46] W. P. Jesse and J. Sadauskis, Phys. Rev. **97**, 1668 (1955), and other recent determinations give $W \geqslant 34$ ev while reference 42 used $W=32.5$ ev.

[47] G. White, National Bureau of Standards Report 1003 (unpublished).

[48] Proceeding of the Photonuclear Conference held at Case Institute of Technology, 1955 (unpublished).

[49] For example, recent determinations of $\int_0^{20} \sigma_{Cu^{63}} dE$ for $Cu^{63}(\gamma,n)Cu^{62}$ are as follows: A. I. Berman and H. L. Brown, Phys. Rev. **96**, 83 (1954): 500 mb-Mev; Scott, Hanson, and Kerst, Phys. Rev. **100**, 209 (1955): 410 mb-Mev; L. Katz and A. G. W. Cameron, Can. J. Phys. **29**, 518 (1951): 660 mb-Mev (this can be reduced to 590 mb-Mev, private communication), V. E. Krohn, Jr. and E. F. Schrader, Phys. Rev. **87**, 685 (1952): 510 mb-Mev.

TABLE IV. Materials modifying the spectrum.

	Element	Amount (g)
Pyrex doughnut wall (3.10 g)	Si	1.12
	O	1.68
	Na	0.09
	K	0.02
	B	0.14
	Al	0.06
Target (0:010 in.)	Pt	0.49

Until these discrepancies are resolved, an uncertainty of about 20% should be assumed for all photodisintegration cross sections.

Solution of Yield Functions

The experimental yields $Y(E_0)$ are related to the cross section $\sigma(E)$, the monitor response $M(E)$ and the effective spectrum $N(E,E_0)$ by the identity

$$Y(E_0)=\int_0^{E_0}\sigma(E)N(E,E_0)dE \Big/ \int_0^{E_0} M(E)N(E,E_0)dE$$
$$=y(E_0)\Big/\int_0^{E_0} MNdE. \qquad (1)$$

If $N(E,E_0)$ were constant for $E=E_0$ and zero for $E>E_0$, direct differentiation of $y(E_0)$ would give the unknown $\sigma(E)$ that is sought. Although the actual $N(E,E_0)$ are not at all of this "block" form, Spencer[50] has shown that it is analytically possible to transform the spectra $N(E,E_0)$ [and the yields $Y(E_0)$] in such a fashion that direct differentiation yields $\sigma(E)$.

In practice, $Y(E_0)$ is obtained only at a finite set of values of E_0, and the necessary operations involve discrete values for the variables and are most conveniently done in matrix form. Suitable matrices have been tabulated by Leiss and Penfold[51]; they are implicitly contained in the tables of Katz and Cameron.

The straightforward application of these methods yields invariably strong oscillations in the derived $\sigma(E)$ values, in particular in the energy region where $\sigma(E)$ is decreasing. As $\sigma(E)$ is believed to be inherently smooth and no physical significance is attached to these oscillations, it has been proposed by Katz and Cameron[49] that $Y(E_0)$, as well as its first and second differences, be smoothed before its conversion to $\sigma(E)$ is attempted.

In the present work, we have preferred another method of smoothing which we shall outline briefly here, relegating details to the appendix. It is based on the fact that $S(E_0)\equiv\int_0^{E_0}\sigma(E)dE$ is always a much smoother function of E_0 than σ is of E. By techniques similar to those discussed above, and indeed using matrices closely

[50] L. V. Spencer, Phys. Rev. **87**, 196 (1952).

[51] A. S. Penfold and J. E. Leiss, Phys. Rev. **95**, 637(A) (1954).

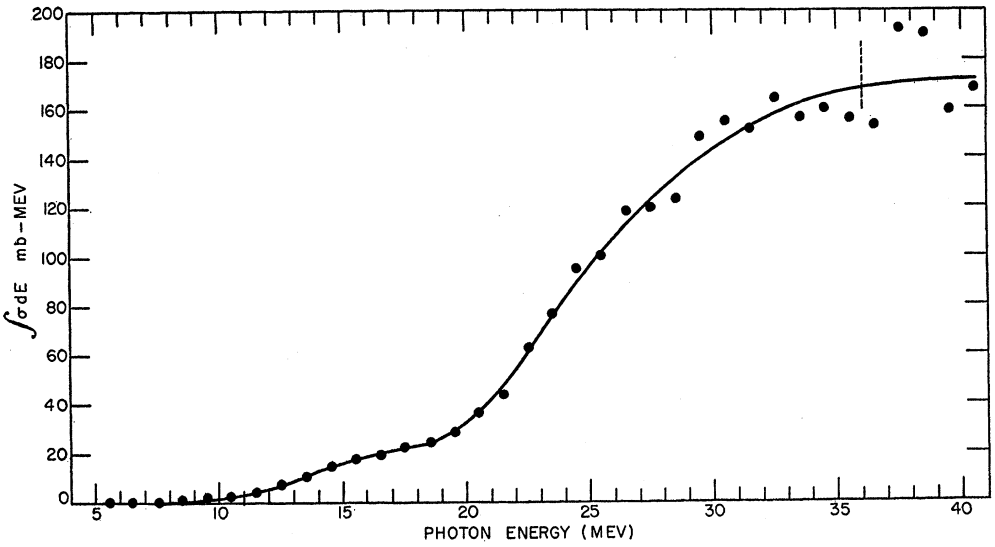

FIG. 10. $\int\sigma dE$ for the C^{13} sample. The points are the direct transformation of the experimental yield points of Fig. 3, "$C^{12}+C^{13}$." The curve is the sum of the derived cross sections $\sigma(E)$.

related to those of Leiss and Penfold, it is possible to obtain $S(E_0)$ directly from $Y(E_0)$. This $S(E_0)$ is then smoothed, and $\sigma(E)$ obtained by differentiation from it. These latter operations were performed as follows: S was expressed near a fixed value of E_0, say E, as a quartic,

$$S(E_0)=\sum_{n=0}^{4} a_n(E_0-E)^n, \qquad (2)$$

the a_n's being obtained by least-squares fitting to 7 points symmetrically about E. Thus $a_n=a_n(E)$, where E goes through the energy range of $Y(E_0)$. By the definition of S, we have $a_1(E)\equiv\sigma(E)$, and the other a_n's need not be computed.

The advantages of this method appear to be: (a) the entire smoothing procedure is analytical and well defined, (b) in principle, it is possible to assign a precise error to each $\sigma(E)$ knowing the errors in the $Y(E_0)$, (c) S, a quantity that is itself of physical interest, is obtained without any smoothing. Incidentally, $\int E^{-1}\sigma(E)dE$, another moment of considerable importance, can similarly be obtained without smoothing.

Figure 10 shows the points for $S(E_0)$ obtained from the (γ,n) yield from the C^{13} sample, indicated in Fig. 3 as "$C^{12}+C^{13}$." The curve in Fig. 10 was obtained by summing the $\sigma(E)$ derived according to the above procedure. The internal consistency of the method is well borne out by this figure.

Cross Sections

The cross sections for $C^{13}(\gamma,xn)$ and $C^{12}(\gamma,xn)$ are shown in Fig. 11, and for $C^{13}(\gamma,p)B^{12}$ in Fig. 12. The $\sigma(\gamma,xn)$ for C^{13} was determined by subtracting the C^{12} contribution to $\int\sigma dE$ and then differentiating. In Table V are listed some relevant threshold values of C^{12} and C^{13}. In Table VI we summarize our results and earlier results for C^{12}.

$C^{12}(\gamma,xn)$.—Our measurement confirms earlier results that the giant resonance peak is at ~22 Mev and narrow. The existence of a high-energy tail is also confirmed.

$C^{13}(\gamma,xn)$.—For $E_0<20.90$ Mev the photoneutron cross section can be attributed to $C^{13}(\gamma,n)C^{12}$ only. $\sigma(\gamma,n)$ for C^{13} exhibits a peak of 3.7-mb height and (5±1)-Mev half-width ($\Gamma_{\frac{1}{2}}$) at (13.3±1.0) Mev. The cross section then goes through a minimum of about 1.8 mb at 17 Mev. This minimum cannot be due to competing processes but is characteristic of σ_{abs} itself. At high energies the cross section increases up to 22 Mev, then dips slightly, reincreases to a peak height of 8.8 mb at 26 Mev and then falls slowly. Above 17.54 Mev the (γ,p) process can influence the $\sigma(\gamma,n)$ by competition and above 20.90 Mev multiple processes become possible. The dip in $\sigma(\gamma,xn)$ and the subsequent reincrease may be attributed to these processes; however, in view of the fact that the allowance made for $\sigma(\gamma,n)$ for C^{12} could be too large and that the analysis used tends to broaden all cross sections, this dip might be spurious. This was the viewpoint taken in our preliminary communication (I). Fortunately no major conclusions that we wish to draw depend critically upon the exact shape of the cross section in this energy region. Since the interpretation of $\sigma(\gamma,xn)$ of C^{13} depends upon the $\sigma(\gamma,p)$ for C^{13}, the latter will be discussed first.

$C^{13}(\gamma,p)B^{12}$.—The $C^{13}(\gamma,p)B^{12}$ as well as $C^{12}(\gamma,p)B^{11}$ cross sections are shown in Fig. 12. The latter cross section is taken from Halpern and Mann.[11] *Note added in proof.*—The $C^{12}(\gamma,p)B^{11}$ cross section has recently been revised. ($\sigma_p=22$ mb) as a consequence at the peak $\sigma_{abs}=29$ mb.¶ The $\sigma(\gamma,p)$ for C^{13} exhibits a peak of

¶ Cohen, Mann, Patton, Reibel, Stephens, and Winhold, Phys. Rev. **104**, 108 (1956).

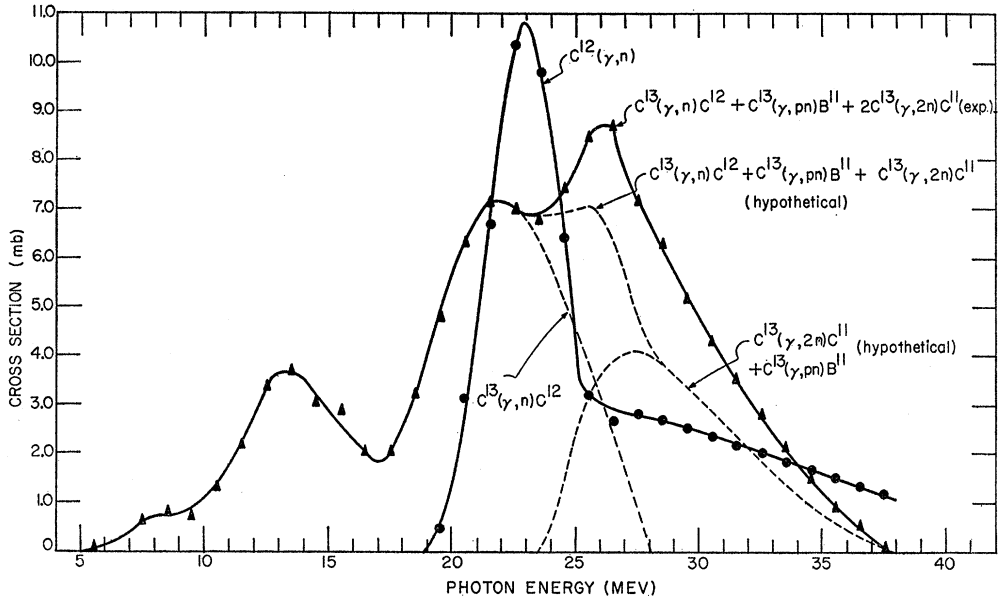

FIG. 11. The cross sections for $C^{13}(\gamma,xn)$ and $C^{12}(\gamma,xn)$. The solid curve is the experimental cross section. The dotted curves for the cross sections $C^{13}(\gamma,n)C^{12}$ and $C^{13}(\gamma,pn)B^{11}+C^{13}(\gamma,2n)C^{11}$ are based on reasonable assumptions about the neutron multiplicity. The curve "$C^{13}(\gamma,n)C^{12}+C^{13}(\gamma,pn)B^{11}+C^{13}(\gamma,2n)C^{11}$ (hypothetical)" is the assumed cross section for all processes yielding neutrons. The assumptions made are discussed in the text.

8.8 mb at 25.5 Mev; in contrast to the $\sigma(\gamma,p)$ for C^{12}, it has a large half-width.

Since it is seen that $\sigma(\gamma,p)$ of C^{13} is large near 22 Mev, the dip in $\sigma(\gamma,xn)$ at that energy might well be real and attributed to proton competition, the (γ,n) process being the main (γ,xn) reaction at this energy. The rise in $\sigma(\gamma,xn)$ at 26 Mev would then be attributed to the (γ,pn) and $(\gamma,2n)$ processes. Similar effects attributed to competition are found in the F^{19}, S^{32}, and P^{31} cross sections.[52,53]

Referring again to Fig. 11, the dashed curve labeled $C^{13}(\gamma,n)C^{12}$ is a conjecture that represents a safe lower limit for this cross section. The difference between this conjectured curve and the experimental curve should then represent $\sigma[C^{13}(\gamma,pn)B^{11}]+2\sigma[C^{13}(\gamma,2n)C^{11}]$ as the neutron multiplicity is two for the second process. Assuming proton and neutron emission to be equally probable, the cross section for multiple-particle production would be two-thirds of this difference. The curve obtained with these assumptions, indicated as "$C^{13}(\gamma,n)C^{12}+C^{13}(\gamma,pn)B^{11}+C^{13}(\gamma,2n)C^{11}$ (hypothetical)," represents our conjecture of the total cross section for processes leading to neutron emission $[\sigma((\gamma,n)+(\gamma,pn)+(\gamma,2n))]$. This estimated cross section follows $\sigma(\gamma,p)$ $(\sigma(\gamma,n)f)$ quite closely above 22 Mev.

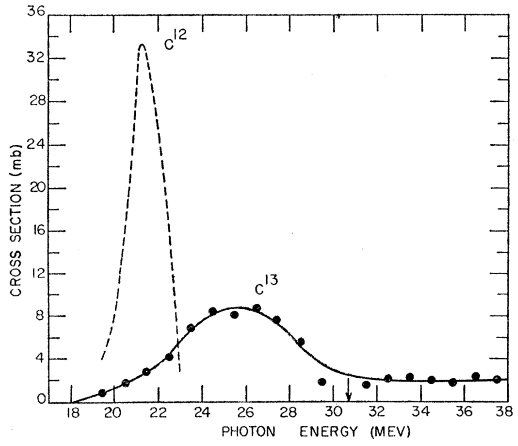

FIG. 12. The $C^{13}(\gamma,p)B^{12}$ cross section. The dotted curve for the $C^{12}(\gamma,p)B^{11}$ cross section is taken from Halpern and Mann (reference 11).

Total cross section σ_{abs}.—$\sigma(\gamma,p)$ and $\sigma((\gamma,pn)+(\gamma,2n))$ can be combined to give an estimate for σ_{abs} as all other modes of decay are expected to be weak above the single particle emission threshold. For C^{13}, σ_{abs} (Fig. 13) exhibits peaks of 3.8 mb and 16 mb at 13.5 Mev and 25 Mev, respectively. Both have large $\Gamma_{\frac{1}{2}}$: (4±1) Mev and (8.5±2) Mev, respectively. σ_{abs} of C^{12} in the energy interval from 19–23 Mev is also indicated in Fig. 13. Below 16 Mev only α or γ emission is possible and above 23 Mev the $\sigma(\gamma,p)$ has not been measured. The contrast in the widths of the high peaks of the C^{12} and C^{13} cross sections is remarkable.

DISCUSSION

In the introduction three main questions concerning the C^{13} cross sections were raised. (1) Are the resonance energies E_r in the photoneutron and absorption cross section of C^{12} and C^{13} the same although the neutron thresholds differ widely? (2) Is σ_{abs} of C^{13} similar to that of C^{12} in the giant resonance region? (3) Can the low-energy cross section of C^{13} be described by a simple model such as used by Guth for the $Be^{9}(\gamma,n)$ cross section?

[52] Taylor, Robinson, and Haslam, Can. J. Phys. **32**, 238 (1954).
[53] L. Katz and A. S. Penfold, Phys. Rev. **81**, 815 (1951).

TABLE V. Thresholds (E_{Th}) for C^{12} and C^{13} photodisintegration processes.[a]

Reaction	E_{Th} (Mev) for C^{12}	for C^{13}
(γ,n)	18.72	4.95
(γ,p)	15.96	17.54
(γ,np)	27.42	20.90
$(\gamma,2n)$	32.04	23.67
$(\gamma,2p)$	27.19	...

[a] From A. H. Wapstra, Physica 21, 367 (1955).

We can on the basis of the present experiment answer as follows:

(1) The resonance energies E_r in $\sigma(\gamma,n)$ and σ_{abs} for C^{12} and C^{13} are approximately the same. This is additional evidence that the observed A dependence of E_r is not accidental,[14] and supports the idea that the giant resonance is a core effect.

(2) The integrals of σ_{abs} over the resonances in C^{12} and C^{13} are approximately equal; however, the detailed shapes of the resonance peaks differ widely. In particular, the width, $\Gamma_{\frac{1}{2}}$ of the giant resonance peak is (8.5±2.0) Mev for C^{13} and (2.5±1.0) for C^{12}. This difference in $\Gamma_{\frac{1}{2}}$ for the neighboring nuclides C^{12} and C^{13} shows clearly how strongly ground-state configurations influence photoabsorption. In fact, since it has been observed that giant resonance is narrow at the closing of the neutron shell $N=50$, the narrow resonance in C^{12} may perhaps be similarly related to the closing of the $P_{\frac{3}{2}}$ shell in $j-j$ coupling.

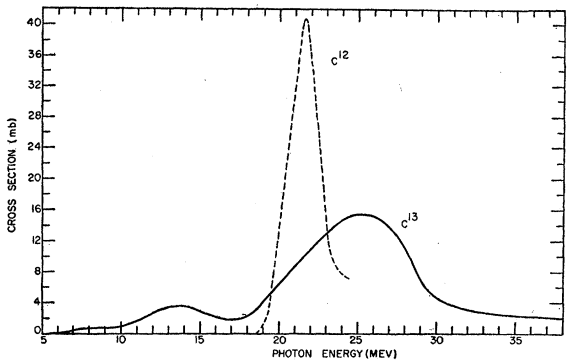

FIG. 13. The total photon absorption cross section for C^{13} and C^{12}.

It should further be pointed out that $\int dE\sigma_{abs}$ over the resonance is in both cases ½ of its sum-rule value while $\sigma_b=\int_0^{38\ Mev}(\sigma_{abs}/E)dE$ is also below its sum-rule limit[54] (~10 mb) [$\sigma_b(C^{12})=4.75$ mb, $\sigma_b(C^{13})=7.54$ mb]. These values are consistent with the systematics of photo-cross sections. It is also seen that $\Gamma_{\frac{1}{2}}$ of C^{13} fits the empirical formula of Halpern, while $\Gamma_{\frac{1}{2}}$ of C^{12} appears to be quite anomalous. The large high-energy tail observed in the σ_{abs} of C^{12} does not appear in the σ of C^{13}. This fact is perhaps related to the narrowness of the C^{12} resonance and need not represent a general feature of the σ for light elements.

(3) While the σ_{abs} of C^{13} exhibits a low-energy peak at 13.5 Mev, the integral $\int_0^{17}\sigma_{abs}dE$ is an order of magnitude too large to be attributed to the single-particle process proposed by Guth and others.[16-17] We first observe that similar peaks are reported in the cross

TABLE VI. Summary of C^{12} and C^{13} photodisintegration data. The limits of integration in the last three columns are given in parentheses.

Experiment		E_p (Mev)	$\sigma(E_p)$ (mb)	$\Gamma_{\frac{1}{2}}$ (Mev)	$\int_{E_1}^{E_2}\sigma dE$ (mb-Mev) (E_1,E_2)	$\int_{E_1}^{E_2}\sigma dE$ (mb-Mev) (E_1,E_2)	$\int_{E_1}^{E_2}(\sigma/E)dE$ (mb) (E_1,E_2)
$C^{13}(\gamma,xn)$	a	24±2	7–9	10±2		70–95(17.38)	
		13.5±1	3.7	5±1	22(5,17)		
$C^{12}(\gamma,xn)$	a	22.8	10.4	3.5	34(18,25)	64–38(18,38)	
	b	22	8.6	3	27	...	
	c	22.5	8.3	4.3	32	56	
	d	21.4	14	2.0	29	...	
	e	22.9	13	2.8	46	...	
	f	...	10	3	48		
	g	23 or 32	...	...	...	86	
$C^{13}(\gamma,p)B^{12}$	a	25.5	8.8	6	55(18,24)		
$C^{12}(\gamma,p)B^{11}$	h	21.5	34	1.8	63(20,24)		
$\sigma_{abs}(C^{13})$	a	25.5±2	16.0	8.5±2	125–140(17,30)		7.54(5,30)
	a	13.5±1	3.7	5±1	22(5,17)		
(C^{12})	a+h	21.5±1	41	2.5±1	100(18,24)		4.75(18,24)

[a] This paper. [b] Reference 2. [c] Reference 5. [d] Reference 1. [e] Reference 45. [f] Reference 10. [g] Reference 9. [h] Reference 11.

[54] L. S. Levinger, Phys. Rev. 97, 122 (1955).

sections[52,55,56] of O^{16}, N^{14}, and F^{19}, and conjecture that such a "pygmy resonance" is perhaps a common feature for all light elements. In addition, if this be true, the absorption is likely to be of $E2$ character, since Spicer has identified the pygmy resonance of O^{16} to be of this type. The difficulty with this interpretation is that $\int\sigma_{\text{abs}}dE$ of C^{13} exceeds the $E2$ sum rule value. This difficulty can be overcome if one assumes a constant $M1$ or $E1$ "background" contribution to the cross section from about 12 Mev to 17 Mev. Then $\int\sigma_{\text{abs}}dE$ over the pygmy resonance would be 5 mb-Mev, consistent with the $E2$ sum-rule. $\Gamma_{\frac{1}{2}}$ for the "true" resonance is then 2.5 Mev. Wilkinson[57] has interpreted the pygmy resonance as the first surface vibrational level of the nucleus. We note that E_r, $\int\sigma_{\text{abs}}dE$, as well as $\Gamma_{\frac{1}{2}}$ of the pygmy resonance of C^{13} are all consistent with this interpretation, although the pygmy resonance may only be a chance grouping of levels in C^{13}. Further work attempting to resolve this resonance would be useful.

In addition to the points mentioned in the introduction, a further question arises: (4) Can statistical arguments alone explain the observed proton/neutron ratio for C^{13}? This question is particularly pertinent here as the observed p/n ratio for C^{12} is correctly predicted by statistical arguments.[4,58] However, for C^{13} the theoretical p/n ratio is only 2.5% if the level densities of B^{11}, C^{11} as estimated in reference 58 are used for B^{12}, C^{12}. We further observe that the density of levels in C^{12} should exceed that of B^{12} (no $T=0$ states exist). Thus the above p/n estimate of 2.5% is certainly an upper limit for the correct statistical estimate. We conclude that statistical arguments fail completely in predicting the observed p/n ratio for C^{13}. Although the correct p/n ratio is given for C^{12}, Wilkinson has shown previously that the observed energy and angular distributions of photoprotons from C^{12} is incompatible with the statistical assumption.[59] His single-particle model for the giant resonance will unambiguously explain the observed p/n ratio for both C^{12} and C^{13}.

ACKNOWLEDGMENTS

I am indebted to Professor C. L. Oxley and Professor H. L. Anderson for the use of the betatron facilities, Dr. W. F. Libby for advice on the chemistry of carbon and use of his laboratory for the target preparation, and Mr. R. Gabriel who assisted in all phases of the experiment. I acknowledge the active participation of Dr. A. S. Penfold in the $\sigma(\gamma,p)$ work, our discussions and his many valuable suggestions. In particular I am indebted to Professor V. L. Telegdi for his guidance and I value his encouragement in this work.

[55] B. M. Spicer, Phys. Rev. **99**, 33 (1955).
[56] Horsley, Haslam, and Johns, Can. J. of Phys. **32**, 238 (1954).
[57] D. H. Wilkinson, Phys. Rev. **99**, 1347 (1955).
[58] H. Morinaga, Phys. Rev. **97**, 1185 (1955).
[59] Mann, Stephens, and Wilkinson, Phys. Rev. **97**, 1184 (1955).

APPENDIX

Conversion of Yields to Cross Sections and Smoothing[60]

Although the transformation method[50] for the solution $\sigma(E)$ of bremsstrahlung yield functions $Y(E_0)$ is not original with us, it has been described as yet only in abstract form. While it is equivalent to the "total spectrum" and "photon difference"[45] methods if applied without smoothing, we shall show that if smooth solutions are sought its use has advantages. We believe that a brief summary of the method is warranted, particularly since the problem of smoothing has not been properly discussed.

The basic integral equation to be solved for σ is

$$Y(E_0)\equiv\int_0^{E_0}dE\sigma(E)N(E,E_0)\exp[-u(E)X]\Big/\int_0^{E_0}dEM(E)N(E,E_0)\exp[-\mu'(E)X']=y(E_0)/m(E_0),\tag{A.1}$$

where σ, N, and M are defined in the text, while μ, μ', and X, X' are the absorption coefficients and thicknesses for attenuation at sample and monitor, respectively. $y(E_0)$ may be called the "reduced yield" and $s(E)\equiv\sigma\exp[-ux]$ the "reduced cross section," and one has the "reduced form of (A.1)":

$$y(E_0)=\int_0^{E_0}dEs(E)N(E,E_0).\tag{A.2}$$

Note that in this form (A.2) is independent of the particular experimental situation. Following Spencer, we operate on both sides with an arbitrary transformation $T(E_0,E')$ such that $T=0$ when $E_0\geqslant E'$ (note also that $N=0$ when $E\geqslant E_0$):

$$\begin{aligned}\tilde{y}(E')&=\int_0^{E'}dE_0y(E_0)T(E_0,E')\\&=\int^{E'}dE_0\int^{E_0=E'}dEs(E)N(E,E_0)T(E_0,E')\\&=\int_0^{E'}dEs(E)\int_0^{E'}dE_0N(E,E_0)T(E_0,E').\end{aligned}\tag{A.3}$$

Defining the transformed spectrum $\tilde{N}$,

$$\tilde{N}(E,E')\equiv\int^{E'}dE_0N(E,E_0)T(E_0,E'),\tag{A.4}$$

[60] A. S. Penfold and J. E. Leiss plan to include a thorough discussion of the matrix method and the assumptions underlying its use as an introduction to their tables of inverted bremsstrahlung matrices (to be published).

we have a transformed yield $\tilde{y}(E')$:

$$\tilde{y}(E')=\int_0^{E'} dEs(E)\tilde{N}(E,E'), \tag{A.5}$$

in complete analogy to (A.2). We choose

$$\tilde{N}(E,E')=\begin{cases}1, & E\leqslant E',\\ 0, & E>E'.\end{cases} \tag{A.6}$$

With this choice of the transformed spectrum $\tilde{N}(E,E')$, we have

$$\tilde{y}(E')=\int_0^{E'} s(E)dE\equiv \mathbb{S}(E'),$$
$$s(E')=d\tilde{y}/dE'=d\mathbb{S}/dE', \tag{A.7}$$

(Note that for $\mu=0$, $\mathbb{S}\rightarrow S$ and $s\rightarrow\sigma$.) The distinction made for rigor between σ, s and $\mathbb{S}$, S will be dropped for convenience hereafter. Thus if $y(E_0)$ is a given analytic function, we obtain a solution $\sigma(E')$. However, in practice $y(E_0)$ is known for a finite number of values of E_0, usually separated by equal intervals, ΔE_0. We therefore replace the above relations for continuous variables by equivalent discontinuous expressions in matrix representation.

$$E_0\rightarrow E_{0n}\equiv n\Delta E_0,$$
$$E\rightarrow E_n\equiv n\Delta E_0-\Delta E_0/2,$$
$$y(E_0)\rightarrow y_n\equiv y(E_{0n}),$$
$$N(E,E_0)dE\rightarrow N_{nm}=N(E_m,E_{0n})\Delta E_0.$$

With these definitions, we have

$$y(E_{0m})=\int_0^{E_{0m}}\sigma(E)N(E,E_{0m})dE\rightarrow \tag{A.2'}$$
$$y_m=\sum_{j=1}^{m} N_{mj}\langle\sigma_j\rangle.$$

We now perform the analog of the transformation (A.4):

$$\tilde{y}_l=\sum_{m=1}^{l} T_{lm}y_m=\sum_{m}^{l}\sum_{j}^{l} T_{lm}N_{mj}\langle\sigma_j\rangle \quad (T_{lm}=0,\ l>m)$$
$$=\sum_{j}^{l}\sum_{m}^{l} T_{lm}N_{mj}\langle\sigma_j\rangle, \tag{A.3'}$$
$$=\sum_{j}^{l}\tilde{N}_{lj}\langle\sigma_j\rangle, \tag{A.5'}$$

where

$$\tilde{N}_{lj}=\sum_{m}^{l} T_{lm}N_{mj}. \tag{A.4'}$$

Penfold and Leiss effectively choose $\tilde{N}_{lj}=\delta_{lj}$ (so that $T=N^{-1}$) to obtain

$$\langle\sigma_l\rangle=\tilde{y}_l, \tag{A.8}$$

whereas we take

$$\tilde{N}_{lj}=\begin{cases}1, & j\leqslant l\\ 0, & j>l\end{cases} \tag{A.6'}$$

so that

$$\tilde{y}_l=\sum_{j}^{l}\langle\sigma_j\rangle=S_l,$$
$$S_l\rightarrow\int\sigma(E)dE. \tag{A.7'}$$

Equations (A.8) and (A.7') give equivalent $\langle\sigma\rangle$ if (A.7') is solved algebraically for $\langle\sigma\rangle$; however if the additional physical requirement is made that $\langle\sigma\rangle$ be a slowly varying function of E' an alternate method is possible using the fact that $\sigma=dS/dE$. From the experimental yield points y_m we first obtain S_l using relation (A.3'). The S_l's are then assumed to approximate a smoothly varying function of E', and $S(E')$ and $\bar{\sigma}$ are determined from S_l by using $\bar{\sigma}=dS/dE'$. (In practice, $\bar{\sigma}$ is expected to be a good approximation to the averaged cross sections, $\langle\sigma_e\rangle$.) $S(E')$ can be differentiated in principle by any standard method. We adopt piece-wise fitting of polynomials to S_l over limited energy intervals to obtain $S(E')$. In view of the resonance-like behavior of $\sigma(E)$, i.e., the fact that inflection points are exhibited, a quartic is a reasonable fitting function for $S(E')$ over a suitably chosen energy interval. Thus we set

$$S(E')=\sum_{j=0}^{4}\alpha_j(E)(E'-E)^j,$$

and have

$$\bar{\sigma}=dS/dE=\alpha_1(E). \tag{A.9}$$

Thus to obtain $\overline{\sigma(E)}$, the $\alpha_j(E)$ with $j\neq 1$ need not be computed. Although the S_j's are not independent, we determine $\alpha_1(E)$ by least-squares fitting at seven points E' about each point E. The resulting σ for any choice of fitting interval will have the form

$$\overline{\sigma_m(E)}=\textstyle\sum_j C_{mj}S_j, \tag{A.10}$$

a linear combination of S_j's.

Actual Computation Procedure

The matrix T used in this analysis is not tabulated, but the problem is readily transformed into one for which the transformation matrix is available. By the trapezoidal rule,

$$\int_0^{E_n} dE\sigma(E)=\sum_{l=0}^{n-1}\sigma_l+\tfrac{1}{2}\sigma_n$$
$$=\sum_{l=0}^{n-1}\frac{\sigma}{E_l}E_l+\frac{1}{2}\frac{\sigma_n}{E_n}E_n$$
$$=\sum_{l=1}^{n-1}\sum_{j}^{l} B_{lj}E_l y_j+\tfrac{1}{2}\sum_{j=1}^{n} B_{nj}E_n y_j, \tag{A.11}$$

where B_{lj} is the matrix tabulated by Penfold and Leiss

$$= \sum_{l=1}^{n-1} E_l \sum_{j=1}^{l} B_{lj}y_j + \tfrac{1}{2}E_n \sum_{j}^{n} B_{nj}y_j$$

$$= \sum_{l=1}^{n} E_l \sum_{j}^{n} B'_{lj}y_j$$

$$= \sum_{j}^{n} T_{nj}y_j.$$

Thus

$$T_{nj} = \sum_{l=1}^{n} E_l B'_{lj}. \qquad \text{(A.12)}$$

(A.12) is an explicit relation between the required matrix T and the tabulated matrix B.

Error in the smoothed cross sections $\bar{\sigma}$.—From (A.10), we have

$$\begin{aligned} \bar{\sigma}_m &= \textstyle\sum_j C_{mj}S_j \\ &= \textstyle\sum_j \sum_k C_{mj}T_{jk}y_k \\ &= \textstyle\sum_k \sum_j C_{mj}T_{jk}y_k, \end{aligned} \qquad \text{(A.13)}$$

$$\Delta^2(\bar{\sigma_m}) = \textstyle\sum_k |\sum_j C_{mj}T_{jk}|^2 \Delta^2 y_k.$$

(A.13) gives the error of σ for given weighting factors C_{mj}.

PHYSICAL REVIEW VOLUME 106, NUMBER 2 APRIL 15, 1957

Relativistic Corrections to p-p Scattering*

G. BREIT
Yale University, New Haven, Connecticut
(Received December 4, 1956)

Effects of wave function distortion by nuclear forces of nonelectromagnetic origin are qualitatively considered. It is found that the relativistic corrections to the Coulomb wave contain effects of wave function distortion which may affect these corrections by reasonably large fractional amounts. The spin-orbit interactions arising from the action of the electric field are found to be affected by wave function distortion. Since these interactions affect the polarization of proton beams in double and triple scattering, the analysis of high-energy data is affected. The theory of spin-orbit interactions is brought into relation with that of atomic spectra. The unreliability of contact terms contained in the relativistic corrections is brought out. A concise proof of the vanishing of first-order tensor force effects on the polarization applying independently of the origin of the tensor force effects is supplied in an appendix.

I. INTRODUCTION AND NOTATION

RELATIVISTIC corrections for p-p scattering have been discussed by Garren,[1] Breit,[2] Ebel and Hull,[3] and again by Garren.[4] The corrections worked out in these papers apply to Coulomb scattering. The viewpoint taken[2] was that specifically nuclear forces introduce phase shifts of their own which can be defined in the center-of-mass system and which require no additional consideration regarding relativistic effects. Two procedures were considered[2] for carrying through the rigorous solution of the problem. Their discussion is contained between Eq. (16.4) and Eq. (17) of the above reference. As an approximation to "procedure (a)" the distortion of the wave function by specifically nuclear interaction effects was neglected and the relativistic corrections to the undistorted Coulomb wave were calculated. Garren's[1,4] approach is equivalent to this approximation. In some of the applications[4] it is tacitly assumed that the approximation is good enough although the question was left open for future consideration in the other work referred to.[2] Further examination shows that specifically nuclear interactions may affect the relativistic corrections to Coulomb scattering to an appreciable degree. This applies in particular to the corrections which matter most for polarization. The quantities involved are large enough to make the application of these corrections to the polarization questionable in any but a qualitative sense. Improvements on the corrections can be made, as will be described below, but a definite value even in the first order of e^2 will be seen to require knowledge of wave functions in the presence of nuclear interactions. It will also be seen that the terms[4] caused by the anomalous part of the proton magnetic moment which have their origin in the divergence of the electric field can be expected to be especially seriously modified. Some of the most frequently occurring symbols used

* This research was supported by the U. S. Air Force through the Air Force Office of Scientific Research of the Air Research and Development Command under Contract AF 18(600)-771 and by the U. S. Atomic Energy Commission under Contract AT (30-1)-1807.

[1] A. Garren, Phys. Rev. **96**, 1709 (1954).
[2] G. Breit, Phys. Rev. **99**, 1581 (1955).
[3] M. E. Ebel and M. H. Hull, Jr., Phys. Rev. **99**, 1596 (1955).
[4] A. Garren, Phys. Rev. **101**, 419 (1956).

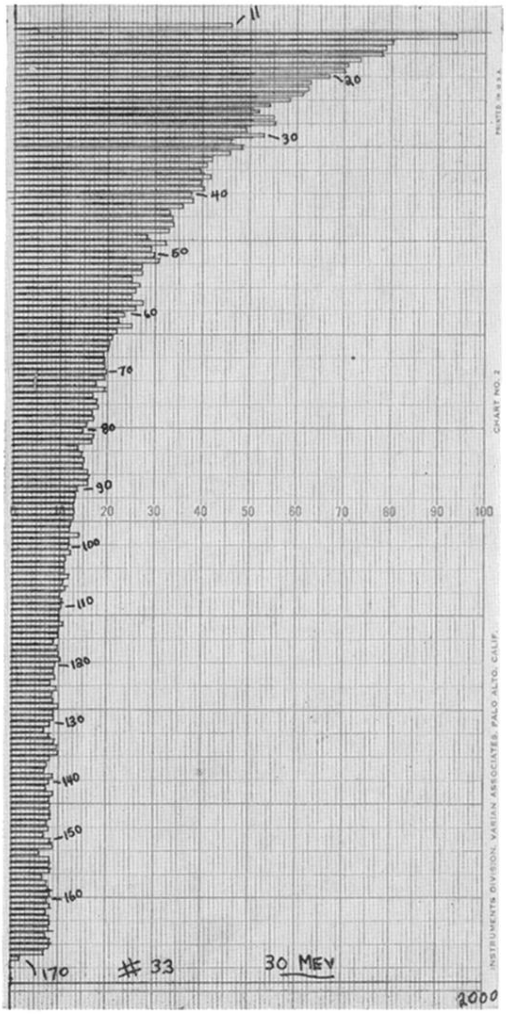

FIG. 5. Reproduction of a typical Varian Record Chart showing number of G-M counts as a function of channel number. (1 channel ≈ 1 msec) Run was taken at $E_0 \approx 30$ Mev. Full scale represents 2000 counts. The separation of the decay into a short-lived component (B^{12}) and a background is apparent.